Research Article

Germanium catalyzed vapor–liquid–solid growth and characterization of amorphous silicon oxide nanotubes: comparison to the growth of its nanowires

Kazuya Hatano[1] · **Keita Kobayashi**[2] · **Takashi Hiraiwa**[1] · **Takatsugu Yoshida**[1] · **Hidehiro Yasuda**[2,3] · **Fumio Kokai**[1]

Abstract

One-dimensional (1D) nanostructures were grown with a simple technique using continuous-wave laser vaporization of a Ge target containing 5 at.% Si in high-pressure (up to 0.9 MPa) Ar gas atmosphere. A maximum amount (~ 30% of all products) of 1D nanostructures was obtained at 0.9 MPa and these nanostructures were identified as amorphous silicon oxide (SiO_x) nanotubes (NTs) and attached with crystalline Ge-rich NPs with elongated prolate-like or sphere-like shapes at their tips by transmission electron microscopy (TEM), high-angle annular dark-field-scanning TEM, and energy dispersive X-ray line scan spectrometry. As the Ar pressure decreased from 0.9 to 0.03 MPa, the average diameters, wall thicknesses, and lengths of the NTs decreased from 57.9 to 22.9 nm, 13.2 to 6.7 nm, and 2.1 to 0.2 μm, respectively, and the tip NP size decreased from 139.0 to 41.7 nm. There was a strong correlation among the diameters, wall thicknesses, and lengths of the NTs and tip Ge NP sizes, indicating the role of molten Ge NPs as catalyst seeds for the precipitation of SiO_x in a vapor–liquid–solid growth mechanism at high temperature. The SiO_x precipitation quantities from the seed NPs for the NTs were compared with those of amorphous SiO_x nanowires (NWs) at 0.1–0.9 MPa to clarify the growth mechanism of the NTs. We argue that smaller precipitation quantities of SiO_x than those for the NWs play a critical role in the formation of cap structures with different sizes and shapes from the molten Ge NPs and the growth of the NTs.

Keywords Silicon oxide · Nanotube · Nanowire · Germanium catalyst · Laser vaporization

1 Introduction

Since the formation of silica (SiO_2) nanotubes (NTs) by Nakamura and Matsui [1] using a sol-gel template method followed by heat treatment, silicon oxide (SiO_x) NTs have attracted great attention due to their fundamental properties and applications in the biotechnology and biomedical fields such as for sensing, separation, and catalysis [2]. Tremendous effort has been devoted to preparing hollow SiO_x NT structures using various templates including anodic aluminum oxide, multi-walled carbon NTs, surfactants, and copolymers [2]. More recently, the templates of polymeric nanowires (NWs) with controlled lengths and diameters of the core and shell were fabricated on a large scale for the precise adjustment of SiO_2 NT structures [3], and new templates of swollen micelles of copolymers were developed to form NTs with widely adjustable inner diameters [4]. In the template-assisted processes, it is relatively easy to form SiO_x NTs with uniform diameters and well controlled lengths and wall thicknesses without the presence of byproducts. However, time-consuming multi-step processes are usually required to form sacrificial templates and SiO_x layers and remove the templates.

In addition to the methods using various templates, several groups developed template-free methods for growing SiO_x NTs. Wang et al. [5] reported the thermal

evaporation of an Si/SiO$_2$ powder at 1400 °C in N$_2$ gas to grow SiO$_2$ NTs. Silicon particles were located the areas that linked the grown SiO$_2$ NTs. Li et al. [6] developed a one-step technique to form ultra-long and well-aligned SiO$_2$ NTs with or without indium (In) filling by heating Si and In$_2$O$_3$ powders. Liquid In was believed to play an important role in the nucleation and growth of the NTs. Liang et al. [7] also reported one-step growth of SiO$_2$ NTs and simultaneous filling with indium sulfide nanorods by heating a Si wafer and In$_2$S$_3$ powders in H$_2$/Ar gas at 950 °C. The combined process of thermal oxidation of Si and low-melting-point In- and S-assisted growth was considered responsible for the NT formation. Hu et al. [8] used the combination of laser ablation of a germanium (Ge) target and thermal evaporation of silicon monoxide (SiO) powders to form various nanostructures based on Si and Ge oxides including SiO$_x$ and Ge-filled SiO$_x$ NTs in an alumina tube furnace. Jiang et al. [9] synthesized SiO$_x$ NTs by using Fe/Co/Ni alloy nanoparticles and heating Si powders in Ar/H$_2$ gas at 1350 °C. Esterina et al. [10] synthesized SiO$_x$ NTs using Co/Pd or Pd thin films on oxidized Si substrates by annealing at temperatures in the range of 650–1050 °C in N$_2$ or N$_2$/H$_2$ gas ambient. The oxidation of growing Si NTs by residual O$_2$ was thought to be important to form SiO$_x$ NTs. Tsuan et al. [11] produced SiO$_x$ NTs from copper sulfide nanocrystals and monophenylsilane in supercritical toluene at 500 °C and 10.3 MPa. The adding of small amounts of H$_2$O and O$_2$ was found to play a critical role in growing the NTs.

In these SiO$_x$ and SiO$_2$ NTs growth, the roles of vapor-liquid-solid (VLS), vapor-solid-solid, and solid-phase seeding processes were suggested involving catalyst metals of In [6, 7], Ge [8], Fe/Co/Ni [9], Co/Pd [10], Pd [10], and Cu [11]. Compared to SiOx NT formation using templates, these template-free methods involve simple one- or two-step procedures; however, the control of NT structures has not necessarily been achieved. Some byproducts coexist and reduce the yield of NTs. For growing a tubular structure, the formation of a cap structure at the edge of a catalyst nanoparticle (NP) seems to be required at the initial stage of growth, while sp^3 bonds dominate a SiO$_x$ structure, unlike carbon NTs constructed by graphene of sp^2 bonds. Important factors, such as the precipitation of an SiO$_x$ sheath from an In droplet under cooling [6], surface dynamics of SiO$_x$ nuclei on the molten Ge droplets such as the wettability of SiO$_x$ with Ge droplets [8], and interface morphology between a seed Cu NP and SiO$_2$ [11] were suggested, while the nucleation process and its effect on SiO$_x$ NT structures to determine their diameters, wall thicknesses, lengths, and so on are not fully understood. We believe that understanding the NT growth mechanism is highly desirable compared with that of the NW growth mechanism for the controlled syntheses of NTs and NWs.

Kokai et al. [12–17] developed a simple growth technique of nanomaterials using continuous wave (CW) laser vaporization of solid targets in high-pressure (up to 0.9 MPa) gas atmosphere. The confinement of atoms and others, such as clusters ejected from the target during their expansion in the gas atmosphere [18], leads to the formation of a high-temperature and high-density growth field. Some one-dimensional (1D) nanostructures, such as Cu- [12] and SiC- [13] filled carbon NTs, SiO$_x$ NWs [14–16], and Ge-carbon core-shell NWs [17] were grown without adding other metal catalysts. In the course of our nanostructure synthesis, we attempted CW laser vaporization of Ge/Si composite targets. From the target of Ge only containing 5–10 atomic (at.) percent of Si, we found that an amorphous SiO$_x$ NT grew while the fraction of the NT was low (up to ~30% in all products). So far, NTs or NWs composed of various elements have been grown by laser vaporization via a VLS mechanism. Usually, targets consisting of large amounts of elements to construct NTs or NWs and small amounts of catalyst metals are used for laser irradiation. For example, single-walled carbon NTs were efficiently formed from the targets of graphite containing small amounts (up to 1.2 at.%) of transition metals [19]. The growth of Si NWs covered with thin SiO$_x$ layers occurred from the target of Si containing 10 at.% Fe [20].

Herein, we focus on the growth of amorphous SiO$_x$ NTs during laser vaporization of a Ge/Si target of an unusual composition in Ar gas under pressures of 0.01–0.9 MPa. The SiO$_x$ NTs with different sizes were grown with sphere- and prolate-like shaped Ge rich NPs at their tips, indicating VLS SiO$_x$ NT growth process involving a Ge molten seed NP. The precipitation quantities of SiOx for the NT growth were tentatively estimated and compared with those for the SiO$_x$ NW growth [14–16]. The main goal of this study is to clarify the nucleation and growth processes of the NTs. Unlike the growth mechanisms of SiO$_x$ NTs in previous studies [6, 8, 11], the formation of cap structures from the molten NPs with different shapes and sizes followed by continuing NT growth is discussed in terms of the quantities of SiO$_x$ precipitation together with considering the times available for maintaining the molten states of seed Ge NPs.

2 Experimental

2.1 Synthesis

Laser vaporization of a Ge/Si composite target (Si content: 5 at.%) was carried out in Ar gas, as reported in previous studies [12–17]. Si powder (Aldrich, 99% purity, 47-μm grain size) was mixed with Ge powder (Aldrich, 99.99% purity and 0.5–147-μm grain size). The mixed powder

was pressed into cylindrical targets (14-mm diameter and 10-mm height) and installed in a stainless-steel chamber. Prior to filling the chamber with Ar gas, the chamber was evacuated to ~ 10^{-1} Pa using a rotary pump and flushed three times with Ar gas. Then, it was filled with Ar gas at pressures ranging from 0.01 to 0.9 MPa. A CW Nd:YAG laser (Lee Laser, Series 800, 1.06 μm wavelength, 500-W output power, and nearly flat-top beam profile) was used for the vaporization of the composite targets at room temperature. The targets were perpendicularly irradiated using the laser beam focused on the target through a quartz window. The laser spot size and power density on the target were adjusted to 2 mm in diameter and about 18 kW/cm^2, respectively, and the laser irradiation time was set to 2 s.

2.2 Characterization

After laser vaporization using a single laser irradiation of 2 s, the deposits produced on the chamber wall were collected and examined using a scanning electron microscope (SEM, Hitachi, S-4800). The deposits were dispersed in an acetone solution using ultrasonication treatment. Then, a drop of the dispersion solution was placed on a Cu plate. After drying, the sample was examined by SEM. The fractions of NTs relative to that of NPs in deposits were different in sampling positions on the chamber wall. The NT fractions were also different in the points in the deposits observed by SEM. So we characterized the deposits by taking several SEM images. Transmission electron microscopes (TEM) operating at 100 kV (Hitachi, H-7000) and 200 kV (JEOL, JEM-ARM200F/UHR) equipped with an energy dispersive X-ray (EDX) spectrometer (JEOL, JED-2300T) were also used to examine the deposits. Similar to the SEM observation of the deposits, a drop of the dispersion solution was put on a Cu microgrid and dried for TEM examination. A Raman spectrum of the deposits was taken using a Raman spectrometer (Jobin Yvon, T-640000M1) with excitation by means of the 488-nm line of an Ar$^+$ laser. Deposits obtained after five laser irradiations were collected and used to measure an X-ray photoelectron (XPS) spectrum on a spectrometer (ULVAC-PHI, PHI Ouantera SXM) using an Al Kα X-ray source. The peak position of the main component in the C 1 s core level spectrum was assumed to be 284.6 eV for calculating the binding energies of each peak.

3 Results and discussion

3.1 Deposit characterization

Figure 1a shows a typical SEM image of deposits obtained from a Ge/Si target at an Ar pressure of 0.9 MPa. 1D
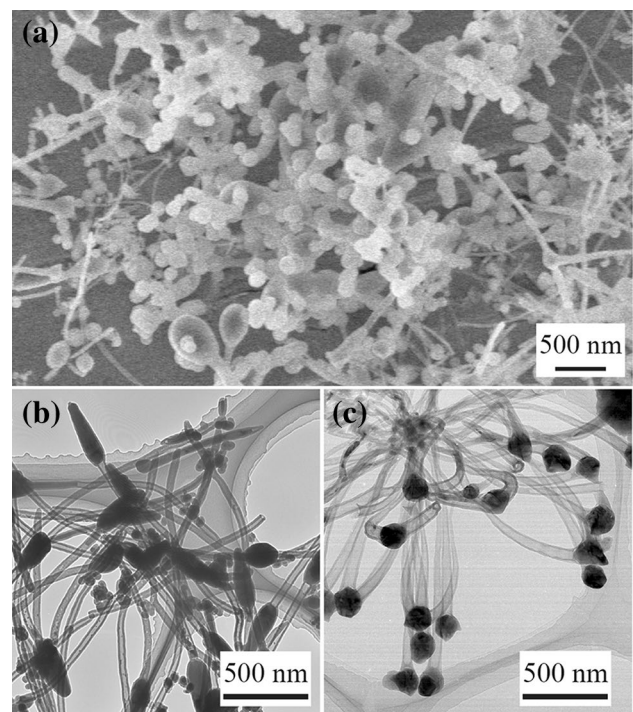

Fig. 1 **a** SEM and **b**, **c** TEM images of products obtained from Ge/Si target at Ar pressure of 0.9 MPa

nanostructures can be seen together with many NPs of sizes from 40–600 nm. These NPs were composed of amorphous SiO$_x$ and GeO$_x$ NPs showing halo selected area electron diffraction (SAED) patterns (Fig. 2). The formation of the 1D nanostructures in all products was dependent on the ambient Ar pressure. The fraction of the 1D nanostructures was estimated from their areas in several SEM images and was maximum (approximately 30%) at 0.9 MPa. Figure 1b and c show TEM images of the 1D nanostructures, which were obtained from the products present in a supernatant fraction of an acetone solution containing the deposits. These TEM images reveal that the 1D nanostructures are hollow NTs of diameters from 30–80 nm and attached with NPs with elongated prolate-like and sphere-like shapes at their tips. The sizes of the two types of tip NP are in the range of 70–400 nm in Fig. 1b and c. Similar type NTs having prolate- or sphere-like NPs were observed as aggregates in the TEM examination. The numbers of the NTs with the two types of NPs attached at their tips were almost the same.

More detailed analysis of the NTs and tip NPs obtained from the Ge/Si target at an Ar pressure of 0.9 MPa was conducted by higher magnification TEM and high-angle annular dark-field-scanning TEM (HAADF-STEM). Figure 3a shows a high magnification TEM image, revealing two amorphous NTs attached with prolate-like NPs at their tips. Figure 3b shows a SAED pattern obtained near the

Fig. 2 **a** TEM image of some NP products revealing different contrasts, **b** high magnification TEM image and **c** the corresponding SAED pattern showing halo for weak contrast NP, **d** high magnification TEM image and **e** the corresponding SAED pattern showing halo for strong contrast NP, EDX spectra of **f** NP seen in **b**, showing peaks assigned to Si and O, and of **g** NP seen in **d**, showing peaks assigned to Ge and O
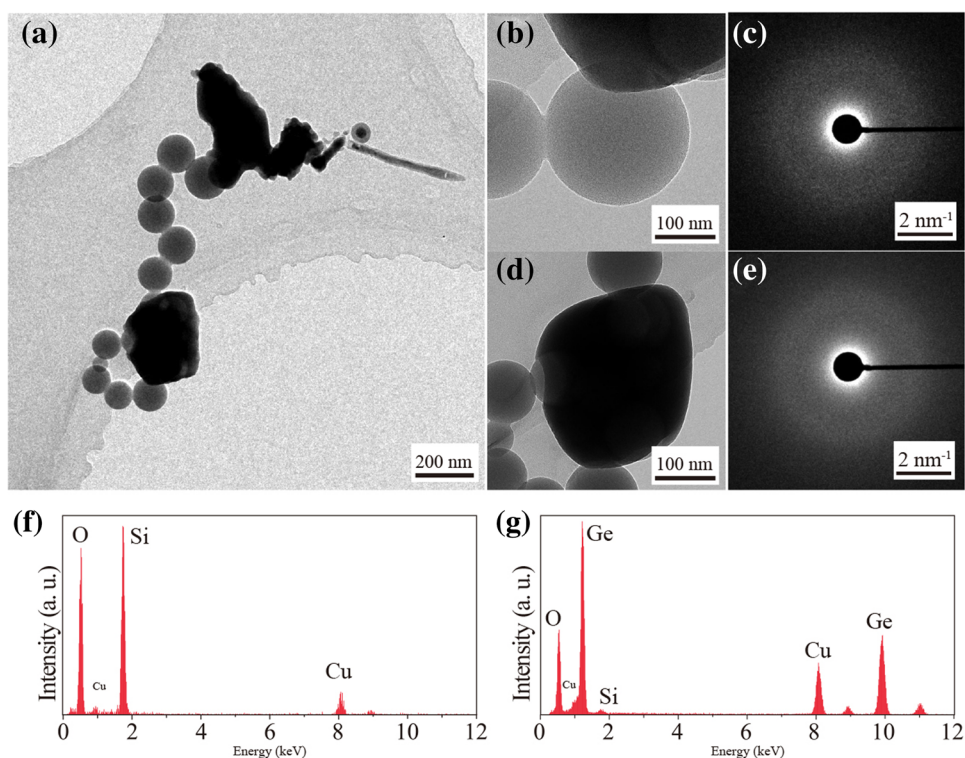

tip portion of the NT present in the lower part of Fig. 3a. The five spots surrounded with red circles are due to the presence of {111} planes of Ge, indicating the tip Ge NP is composed of a polycrystalline Ge. Figure 3c is a high-resolution (HR) TEM image of the part surrounded with a red square in Fig. 3a, revealing the presence of lattice fringes corresponding to the distance (0.3266 nm) of diamond-type crystalline Ge (JCPDS:004-0545) and an amorphous layer covering the Ge NP. Figure 3d shows a HAADF-STEM image of the NTs and prolate-like tip NPs shown in Fig. 3a. Tip Ge NPs with strong contrast and NTs and NP covering layers with weak contrast can be seen. Figure 3e, f shows EDX line scan profiles at the tip NP and NT, respectively. The strong signal from a Ge atom was detected in the tip NP and weak signals from Si and O atoms were detected at the edges of the tip NP. On the other hand, signals from Si and O atoms were only detected in the NT portion. The Ge signal was maximized when beam is positioned in center of tip NP and attenuation of the Si and O signals was clear when beam was positioned in center of NT, which was consistent with morphologies of the NP and hollow NT. The atomic ratio of O relative to Si (O/Si) was determined from the intensities in the EDX profile of the NT. The average O/Si was about 1.9 from the three positions of the NT and was close to that of SiO_2.

The examination of TEM and HAADF-STEM images was also conducted for NTs attached with sphere-like NPs (Figs. 4 and 5). A fast Fourier transform pattern displays

sharp spots indicating presence of crytalline Ge and a HRTEM image reveals the presence of lattice fringes corresponding to lattice distances (0.3266 nm) originated from {111} planes of crystalline Ge. In a HAADF-STEM image, a tip Ge NP with strong contrast and a NT and a NP covering layer with weak contrast are seen. The intensity distributions of Ge, Si, and O atoms along the position in both the tip NP and NT in EDX line scan profiles are consistent with the morphologies of the NP and NT, similar to those for the NTs attached with prolate-like NPs. These findings indicate that the NTs are composed of amorphous SiO_x and the tip NPs are composed of polycrystalline Ge covered with amorphous SiO_x layers. In addition to the SiO_x NTs, NWs composed of a core-shell structure with a Ge core and SiO_x shell were also formed (Fig. 6), as also seen in the upper and left parts of Fig. 1b. However, the fraction of the core-shell NWs was small (1–2%) in all products.

Both the diameters and wall thicknesses of SiO_x NTs attached with prolate- and sphere-like NPs were measured at a distance of ~20 nm from tip NPs for each 100 samples, as respectively shown in Figs. 7 and 8. The ranges of the diameters and wall thicknesses were 20–120 nm and 6–24 nm, respectively. The diameters and thicknesses of the NTs attached with prolate-like NPs tended to be smaller than those attached with sphere-like NPs. The average diameters and wall thicknesses were 51.6 and 12.6 nm for NTs attached with prolate-like NPs and 64.1 and 13.7 nm for those attached with sphere-like NPs.
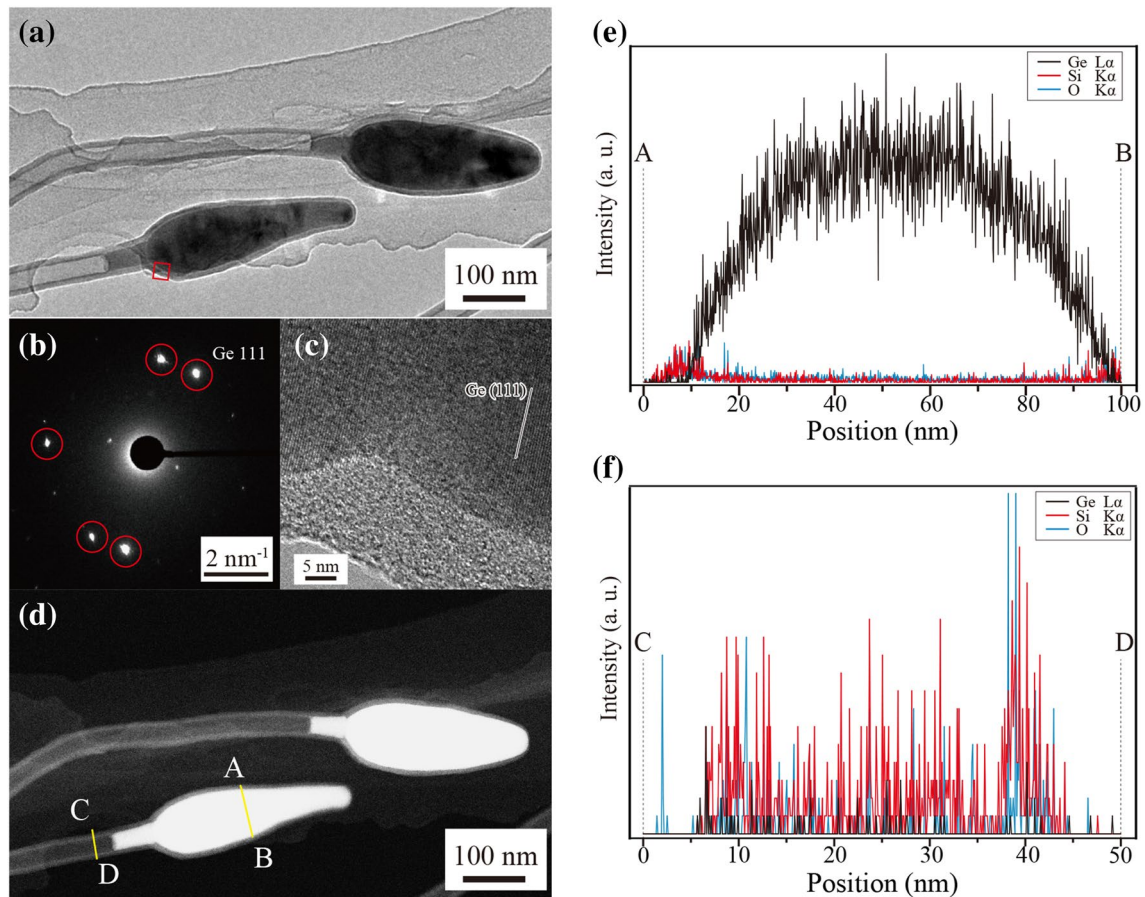
Fig. 3 **a** High magnification TEM image of two NTs attached with prolate-like NPs at their tips, **b** SAED pattern, **c** HRTEM image of part surrounded with red square in **a**, **d** HAADF-STEM image of two NTs attached with prolate-like NPs, and EDX line scan profiles at **e** tip NP and **f** NT

The deposits obtained from the Ge/Si target at an Ar pressure of 0.9 MPa were also analyzed by XPS and Raman spectroscopy (Figs. 9, 10). In the wide scan XPS spectrum (Fig. 9a), peaks assigned to Ge 3d, Si 2p, C 1s, O1s, and so on are seen. In the Ge 3d spectrum (Fig. 9b), two peaks are observed at 29.4 and 32.8 eV and assigned to the component of Ge bonded to Ge or Si and the component of oxidized Ge atoms [21] An O 2s peak overlapped with peak at 29.4 eV is frequently observed in samples containing SiO_x [22]. The Si 2p spectrum reveals peak at 103.3 eV indicating presence of SiO_x [23] Broad O 1 s peak (full width of half maximum of 2.3 eV) at 532.3 eV probably consists of two components of O bonded to Ge (~ 531.9 eV) or Si (~ 532.6 eV) [24, 25] The presence of metallic and oxidized Ge and oxidized Si was confirmed in the deposits. The Raman spectrum (Fig. 10) of the deposits shows a strong band at 294 cm^{-1} and a weak band at 393 cm^{-1} attributed to Ge-Ge and Ge-Si modes, respectively, as seen in the Raman spectra of alloys [26] and NWs [27] of crystalline $Si_{1-x}Ge_x$. The two bands observed in this study are probably due to the presence of crystalline Ge NPs and the

interfaces of Ge and SiO_x in tip NPs. Thus, the results of XPS and Raman spectra are consistent with the analysis of the products based on SEM and TEM.

3.2 Effect of Ar pressure

The change in the ambient Ar pressure significantly affected the growth behavior of the SiO_x NTs. Figure 11 shows TEM images of products obtained at Ar pressures of 0.5, 0.1, 0.05, 0.03, and 0.01 MPa. As the Ar pressure decreased, NTs tended to be thinner and shorter and with attached smaller NPs, as seen in Fig. 11a–d. In addition, the fractions of the NTs in all products decreased to ~ 20% at 0.5 MPa, ~ 10% at 0.1 MPa, ~ 3% at 0.05 MPa, and ~ 1% at 0.03 MPa. As only the aggregates of small NPs are present in the TEM image of Fig. 11e, no NTs were observed in the deposits obtained at an Ar pressure of 0.01 MPa. These findings indicate the remarkable effect of Ar pressure on the growth and size of NTs.

Figure 12 plots the average diameters, wall thicknesses, and lengths of SiO_x NTs and average sizes of tip NPs at Ar

Fig. 4 **a** TEM image of NT attached with sphere-like NP, **b** HRTEM image of part surrounded with red square in **a**, **c** fast Fourier transform pattern corresponding to **b**, and **d** HRTEM image of part surrounded with yellow square in **b**
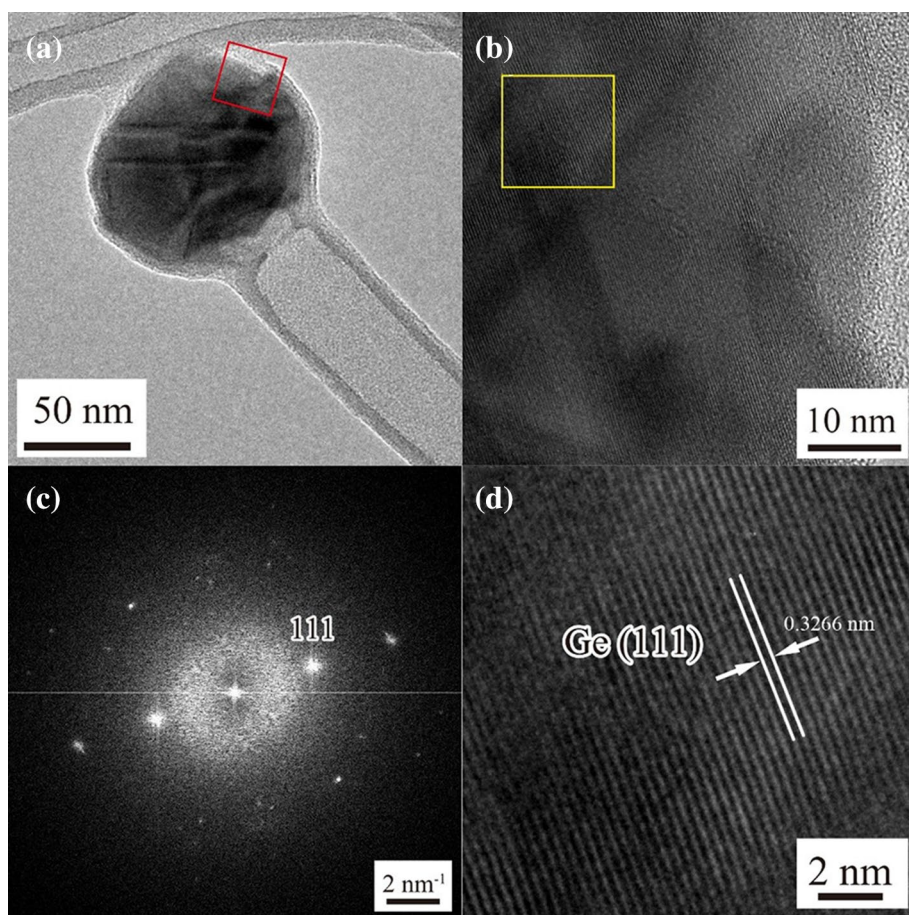

Fig. 5 **a** HAADF-STEM image and EDX line scan profiles at **b** sphere-like tip NP and **c** NT
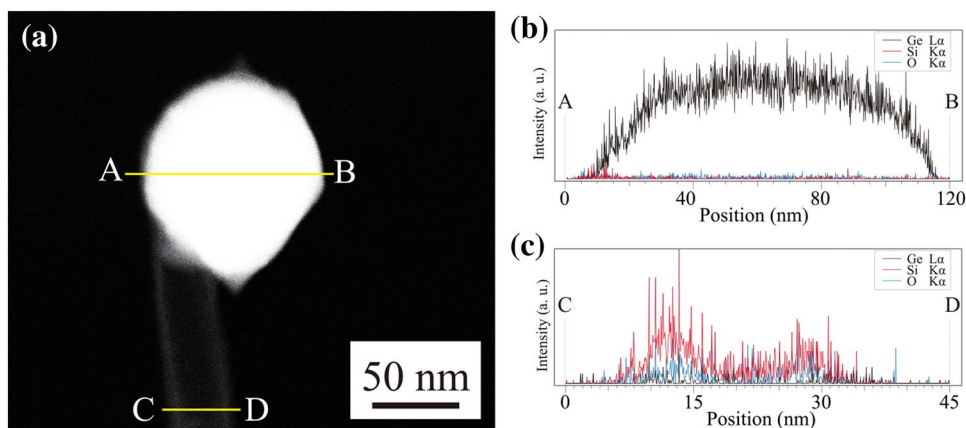
pressures of 0.03, 0.05, 0.1, 0.5, and 0.9 MPa. The average sizes of the attached NPs with prolate- and sphere-like shapes were determined from measuring the maximum lengths of the NPs perpendicular to the growth direction of NTs, i.e., the lengths of short axes for most of the prolate-like NPs. As the Ar pressure decreased from 0.9 to 0.03 MPa, the average diameters decreased from 57.9 to 22.9 nm, the average wall thicknesses decreased from 13.2 to 6.7 nm, the average lengths decreased from 2.1 to
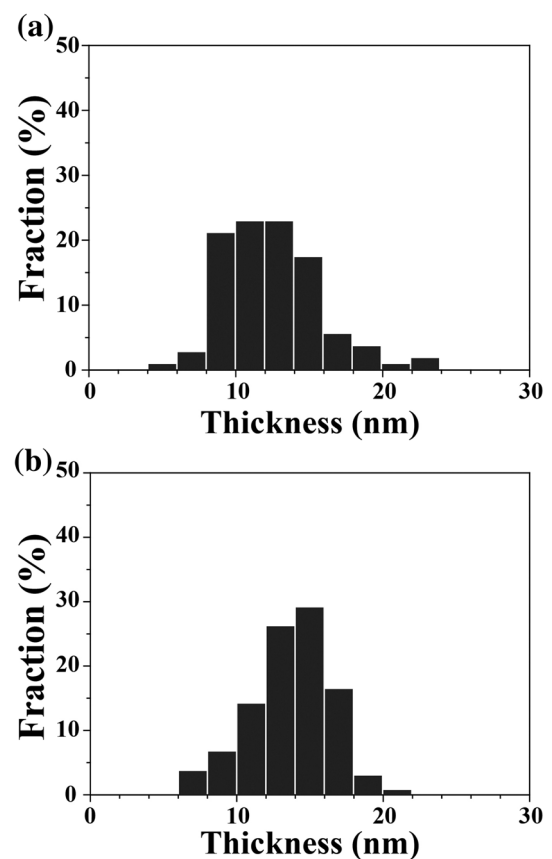
0.2 μm, and the average tip NP sizes decreased from 139.0 to 41.7 nm. These four plots exhibit very similar curves, indicating the strong correlation among the average diameter, wall thicknesses, and lengths of SiO_x NTs and the average sizes of tip NPs. Interestingly, the ratios of the average wall thicknesses relative to the average diameters obtained at 0.03–0.9 MPa were almost constant (~24%) (Fig. 13). The strong correlation probably resulted from certain factors including the role of tip Ge NPs as seeds

Fig. 6 **a** TEM and **b** HAADF-STEM images of core–shell NWs simultaneously grown with SiO_x NTs. The strong and weak contrasts in parts of core and shell indicate formation of Ge–SiO_x core-shell NWs
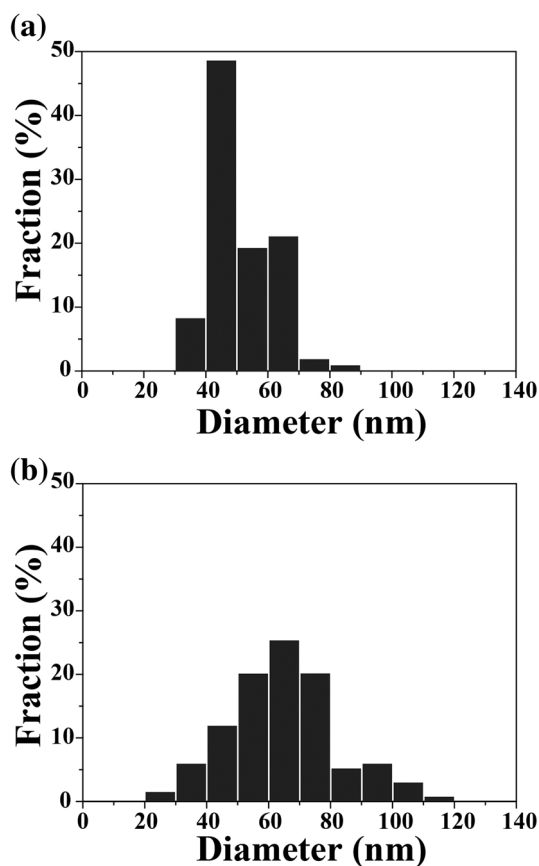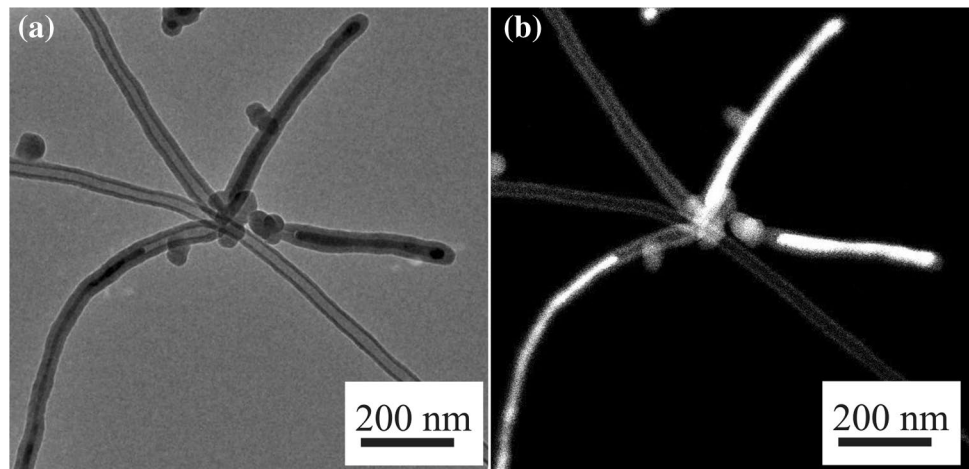
**Fig. 7** Histograms of diameters of SiO_x NTs attached with NPs of **a** prolate- and **b** sphere-like shapes

Fig. 8 Histograms of wall thicknesses of SiO_x NTs attached with NPs of **a** prolate- and **b** sphere-like shapes

for growth of SiO_x NTs and precipitation quantities of SiO_x from the seeds, as mentioned below. Furthermore, in each plot, the large changes in the average values occurred at lower Ar pressures between 0.03 and 0.1 MPa. This behavior may relate to the decrease in ejected Ge and Si species from the Ge/Si target at higher pressures, as was the

depression of etching of polymer films in pressurized He and N_2 gas ambients up to 15 MPa [28]. We also observed a decrease in crater depth in the Ge/Si targets as the Ar pressure increased. The values of weight loss in the targets (3 g in original weight) after single laser irradiation were measured to be about 0.59, 0.56, and 0.52 g for 0.1, 0.5, and 0.9 MPa.
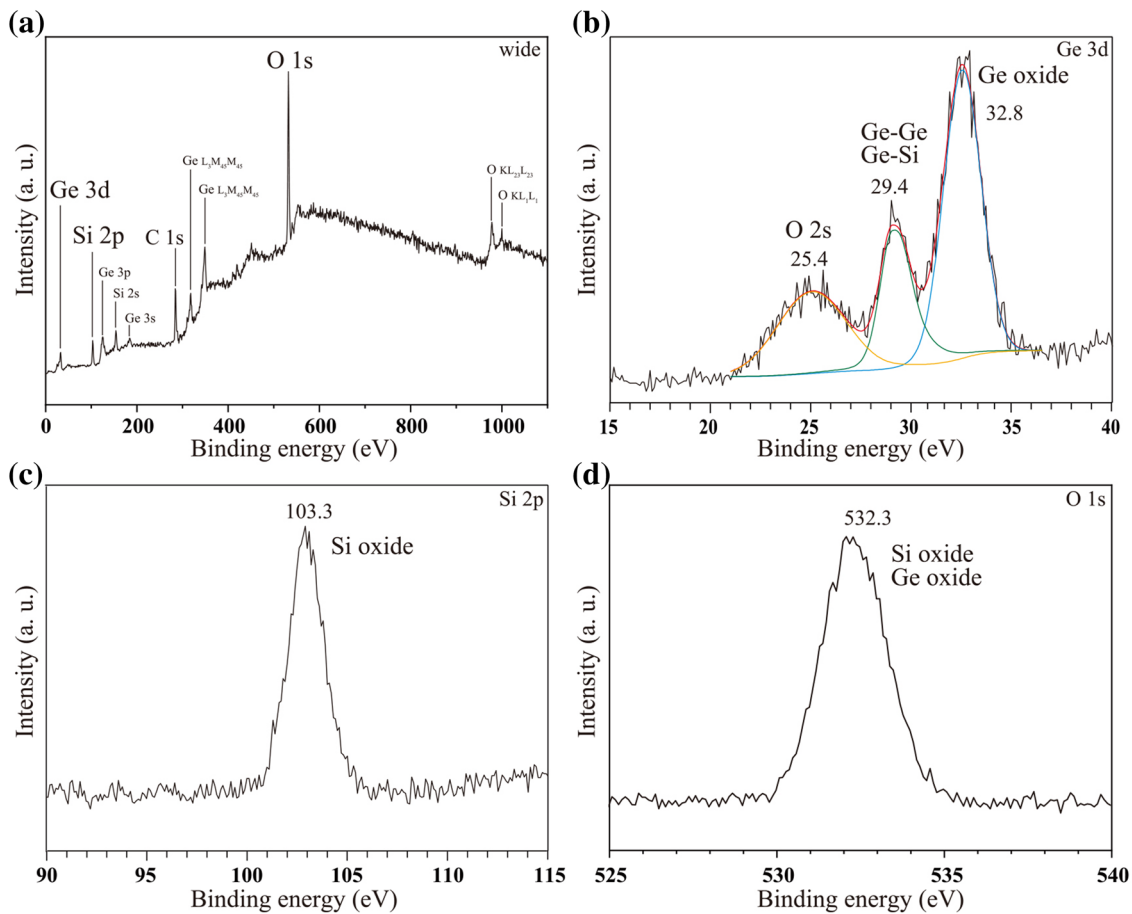
Fig. 9 **a** Wide scan, **b** Ge 3d, **c** Si 2p, and **d** O 1s XPS spectra of deposits obtained at 0.9 MPa
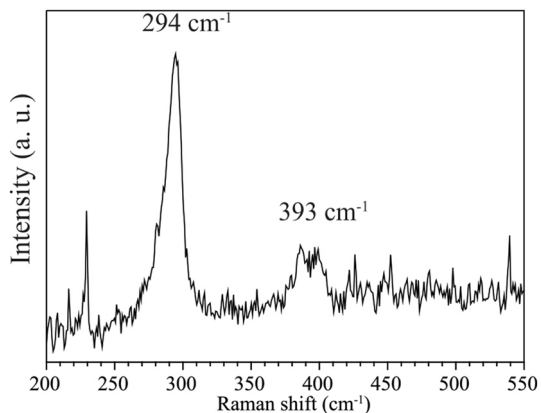

Fig. 10 Raman spectrum of deposits obtained at 0.9 MPa

3.3 Growth process of SiO$_x$ NTs

Let us discuss the growth process of the SiO$_x$ NTs. The existence of tip NPs of Ge covered with SiO$_x$ layers and the strong correlation of the NT diameters, wall thicknesses, and lengths with the tip NP sizes suggest that the SiO$_x$ NTs were grown via a VLS mechanism involving liquid-like molten Ge NPs as seeds. Hu et al. [8] reported the catalytic activity of Ge for the growth of SiO$_x$ and Ge-filled SiO$_x$ NTs occurred on an Si substrate, in which hollow NTs with diameters of 80–150 nm and a wall thickness of 40 nm coexisted with Ge-filled NTs. Unlike their growth method using a combination of laser vaporization of a Ge target and thermal evaporation of SiO powders for 4 h in a high-temperature furnace, we observed SiO$_x$ NT growth as a result of a single event after 2-s CW laser irradiation onto a Ge target containing 5 at.% Si in Ar atmosphere at room temperature. We believe that our NT growth occurs in a gas phase as is the growth of carbon nanohorns and NTs by laser vaporization of graphite and graphite containing a small amount of Co/Ni in Ar atmosphere [29, 30], in which their growth dynamics were studied using shadowgraphy and emission imaging. After the CW laser irradiation onto the Ge target containing 5 at.% Si, an important stage is the formation of Ge-rich molten NPs at high temperature based on Ge and Si atoms and others such as clusters ejected from the target. The source of the O atoms could have several origins such as residual O$_2$ in
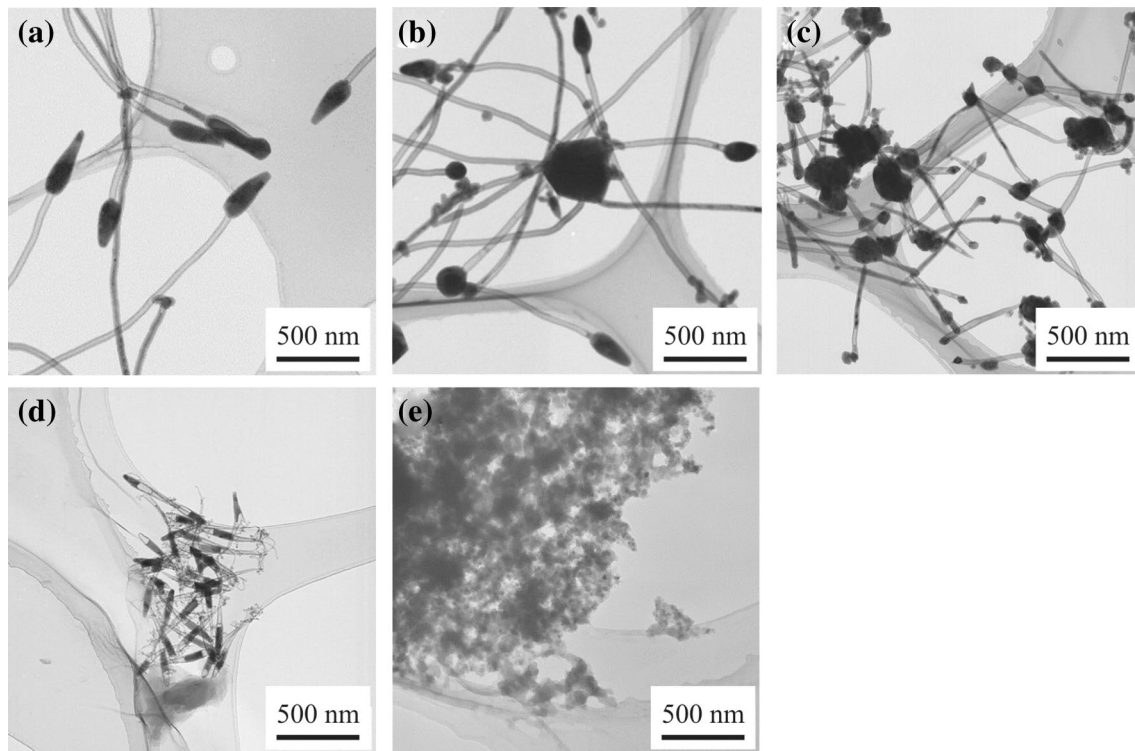
Fig. 11 TEM images of products obtained at Ar pressures of **a** 0.5, **b** 0.1, **c** 0.05, **d** 0.03, and **e** 0.01 MPa

the stainless-steel chamber, H_2O and O_2 in the Ar gas, or natural oxidation layers present on the surfaces of the Si and Ge powders [15].

The degree of confinement of the ejected species from the target, growing clusters, and molten Ge-rich NPs by surrounding Ar strongly affects the sizes of the molten Ge-rich NPs dependent on Ar pressure. The tip NP sizes in Fig. 12d indicate that the sizes of the molten Ge-rich NPs increased with increasing Ar pressure from 0.03 to 0.9 MPa. The degree of confinement also affected the maintaining of high temperature of the growing clusters and molten NPs and decreased their temperature gradients to room temperature [29, 30]. The confinement by Ar leads to collisional heating, resulting from the conversion of kinetic energies of the clusters and/or NPs into thermal energies [30] in addition to the cooling process of the clusters and molten NPs by the collision with Ar. More rapid decrease in temperature occurs in lower pressure Ar, as estimated from the blackbody temperature in the laser vaporization of graphite [29].

The formation of the crystalline Ge-rich NPs with prolate- and sphere-shapes, observed as final products after cooling, probably results from the difference in the temperature gradient during Ge crystallization. Since the fraction of the NTs with prolate-like NPs attached at their tips increase with decreasing Ar pressure, they are thought to be formed in steeper temperature gradients.

The solidification behavior of Ge microdroplets was reported in the size range from 200 to 500 µm, which was produced using a pulsated orifice-ejection method [31]. Corresponding to two ejection temperatures of 1220 and 1370 K, two shapes, lemon- and grapefruit-like ones, of crystalline Ge particles were observed, and their formation was explained by the different behaviors in crystallization.

The deformation of molten Ge-rich NPs may occur during the growth of SiO_x NTs at high temperature, as observed for Ni seeds involved in the growth of carbon NTs [32] However, from the observed difference in SiO_x NT diameters and tip NP shapes (Figs. 1b, c, 3a, 4a, 11a–d), the molten Ge NPs with different shapes, which are close to the prolate- and sphere ones, are considered to contribute to SiO_x NT growth, while exact shapes of molten Ge NPs probably affected by its surface tension such as other metals for the reported Si NW growth [33] are not known. The growth occurs through the supply of Si and O species to the molten Ge-rich NPs, their diffusion in and/or on the NPs, and the precipitation of SiO_x from the NPs by supersaturation of SiO_x. Due to the much higher binding energy of Si-O (799.6 kJ/mol), compared to those of Ge-O (657. 6 kJ/mol), Ge-Si (297 kJ/mol), and Si-Si (310 kJ/mol) [34], solid SiO_x is thought to preferentially precipitate from the edges of the molten Ge-rich NPs. As long as the temperature is high enough to maintain the molten states of the Ge-rich NPs, SiO_x precipitation continues.
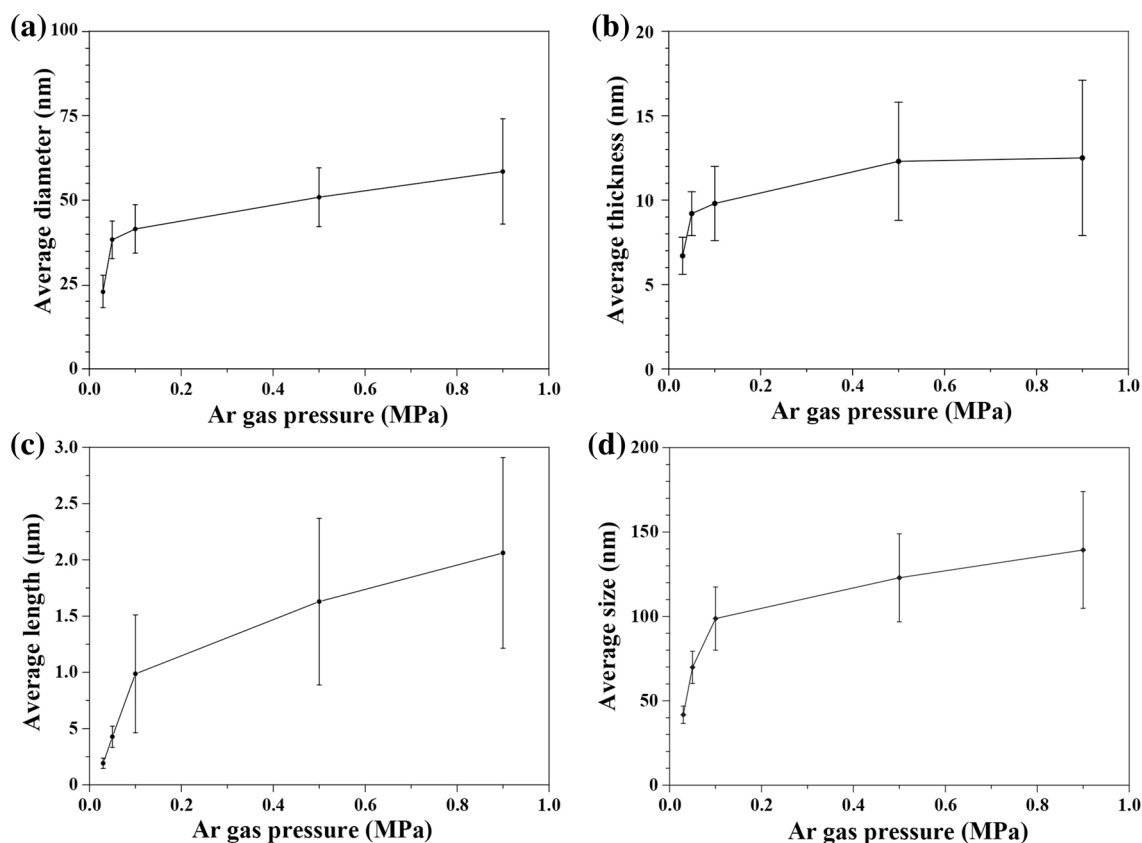
Fig. 12 Averages of **a** diameters, **b** wall thicknesses, and **c** lengths of SiO_x NTs and **d** average sizes of tip NPs as function of Ar pressure. Plots for 0.9 MPa were based on each of 100 samples of NTs attached with prolate- and sphere-like NPs. Plots for 0.5, 0.1, 0.05, 0.03 MPa were based on each of 30 samples of NTs and tip NPs. Error bars at each plot are standard errors

3.4 Comparison of growth mechanisms of SiO_x NTs and NWs

For hollow SiO_x NT growth, the formation of a cap structure
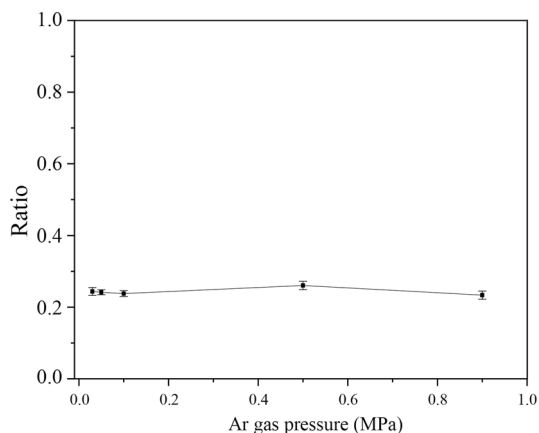
Fig. 13 Ratios of SiO_x NT wall thicknesses relative to NT diameters obtained from each average value at 0.03, 0.05, 0.1, 0.5, and 0.9 MPa

seems to be essential on the molten Ge-rich NP at a nucleation stage of the NT. How is the cap structure formed? We believe that the growth of the NTs with different diameters and walls thicknesses (Figs. 7, 8, 12a, b) occurs from the formation of caps with different sizes in Ar atmosphere under pressures from 0.03–0.9 MPa. We tentatively compared two SiO_x precipitation processes leading to the growth of NTs and NWs of SiO_x by high-pressure CW laser vaporization. The amorphous SiO_x NWs, up to 4 μm long [14] and O/Si of 0.8–2.0 [15] with Si NPs attached at their tips were grown in Ar atmosphere under pressures of 0.1, 0.5, and 0.9 MPa from targets of Si and its oxides [14–16]. Although the catalytic activities of Ge and Si molten NPs are different for NT and NW growth, we believe that certain important aspects leading to NT or NW growth should be involved. Figure 14a plots the volumes of the 100-nm-long NTs and NWs calculated from the average diameters and wall thicknesses of the NTs (Fig. 12a, b) and from the average diameters of the NWs [14]. The NW volumes largely increase from 1.0×10^{-17} to 7.2×10^{-17} cm^3 at 0.1–0.9 MPa, corresponding to the growth of the NWs with larger diameters at higher Ar pressures. However, the NT volumes slightly increase

(a)

(b)
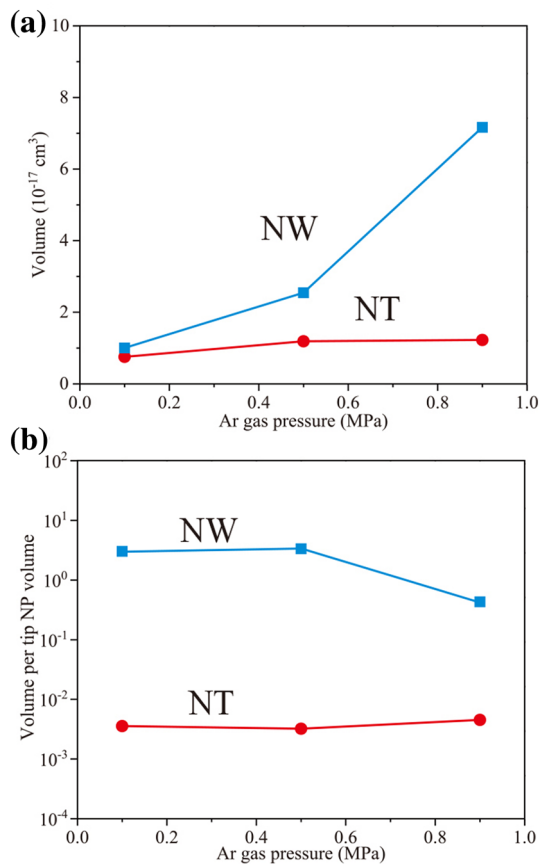
Fig. 14 **a** Volumes of 100-nm-long SiO_x NTs and NWs obtained at 0.1, 0.5, and 0.9 MPa and **b** volumes of 100-nm-long SiO_x NTs and NWs divided by volumes of tip NPs. 100-nm-long NT volumes were calculated from their average diameters (41.5, 50.9, and 57.9 nm) and wall thicknesses (9.8, 12.3, and 13.2 nm) shown in Fig. 12a, b. Volumes of 100-nm-long NTs were calculated from average diameters of NWs of 11.3, 18.0, and 30.2 nm [14]. For calculation of volumes of SiO_x NTs per tip NP volume, ratios of prolate-like tip particles were assumed to 80, 70, and 50% at 0.1, 0.5, and 0.9 MPa, and their shapes were assumed to be ellipsoid. Lengths of two short axes in ellipsoids were assumed to be average sizes (98.7, 122.9, and 139.0 nm) in Fig. 12d, and lengths of long axes were assumed to be three times of those of two short axes. For calculation of SiO_x NW volumes per tip NP volume, tip NP diameters of 18.5, 24.4, and 68.2 nm [14] were used

from 0.8×10^{-17} to 1.2×10^{-17} cm^3 at 0.1–0.9 MPa. As the Ar pressure increased, the NTs with larger diameters and wall thicknesses were grown (Fig. 12a). The slight increase is due to the hollow structures of the NTs. The NT volumes are 17–75% of the NW ones at 0.1–0.9 MPa.

In addition to the NT and NW volumes, we also estimated the NT and NW volumes per volume of the tip NPs, as shown in Fig. 14b. There is no clear tendency in the relative volumes of the NWs and NTs as the Ar pressure changes. The relative NW and NT volumes are 0.43–3.0 and 3.2×10^{-3}–4.5×10^{-3}, respectively. The relative volumes at different Ar pressures may be affected by certain
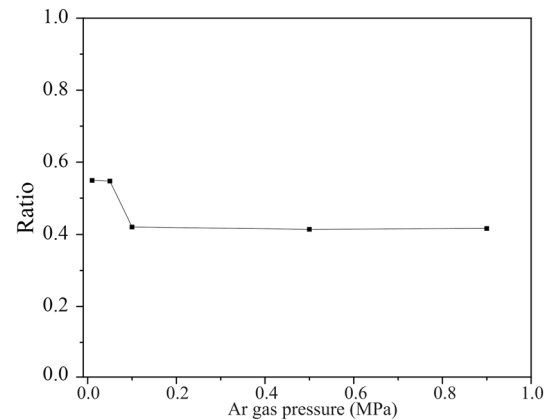
Fig. 15 Ratios of SiO_x NT diameters relative to tip NP sizes obtained from each average value at 0.03, 0.05, 0.1, 0.5, and 0.9 MPa. Larger ratios at lower Ar pressures may results from higher degree of SiO_x supersaturation

complicated factors, such as growth temperatures, supply rates of SiO_x to the molten Ge NPs, diffusion rates, and degree of supersaturation of SiO_x in and/or on the Ge NPs. The degree of supersaturation may be larger at lower Ar pressures, resulting in the growth of larger diameter NTs relative to those of tip NPs (Fig. 15), i.e., the growth of NTs with larger precipitation volumes, as suggested with SiO_x NW growth [16]. If the growth of SiO_x NTs occurs in a narrow temperature range, the diffusion rate of SiO_x may be similar. Therefore, the relative NT and NW volumes at 0.1, 0.5, and 0.9 MPa seem to be determined by various factors. Accordingly, we focus on the large differences between the relative NW and NT volumes. In Fig. 14b, the NT volumes are 1.2×10^{-3}–1.0×10^{-2} of those of the NWs. Therefore, we believe that smaller SiO_x precipitation leads to NT growth. The smaller SiO_x precipitation probably results from the supply of less Si and O species to the molten Ge NPs and their slow diffusion in and/or on the NPs. The difference in SiO_x solubility between Ge and Si NPs may also be related to each SiO_x precipitation quantity. The SiO_x NT growth only occurred when using Ge/Si targets with unusual compositions (Si content: 5–10 at.%), leading to the supply of a limited amount of Si species to the molten Ge NP. From the analysis involving the Si 2p XPS spectrum (Fig. 9), almost all Si atoms present in the products appeared to bond with O atoms. The quantity of SiO_x formed from Si in the target and from O_2 probably in residual gas may be suitable for the SiO_x NT growth under the condition of the small precipitation of SiO_x. The continuation of the precipitation process for a certain time results in the formation of NTs with lengths of up to ~3 μm.

The NT growth occurs from the molten Ge NPs with different shapes and sizes judging from the TEM images (Figs. 1b, c, 3a, 4a, 11a–d) and the curvature of the molten

Ge NPs, affected by Ge surface tension, seems to be related to determining the diameters and wall thicknesses of the NTs. However, the curvature does not seem to directly govern the occurrence of NT or NW growth. Although we only analyzed final products without in situ observation of NT and NW growth, we propose that small SiO_x precipitation quantity at the nucleation stage plays a critical role in the formation of a cap structure, for example, by the separation of a SiO_x sheath from a molten Ge NP. Under the condition of the small SiO_x precipitation quantity, the reason for preferring the formation of a tube structure to avoid a thin wire structure is not clear. However, some factors such as a low SiO_x diffusion rate in and/or on a molten Ge NP and its temperature gradient and deformation may contribute to the cap structure formation. Once the formation of the cap structure occurs, SiO_x precipitation continues, resulting in an elongated NT structure, due to stable interface energy between a liquid Ge NP and a solid SiO_x NT like Si NW formation [33].

3.5 Time available for SiO_x NT growth

Finally, we discuss the times available for our SiO_x NT growth in Ar atmosphere under different pressures, which strongly affect the NT lengths. In relation to the growth of carbon nanohorns and NTs, emission from growing clusters and/or condensing NPs were observed during the laser vaporization of graphite and graphite containing 1.2 at.% of Co/Ni using laser irradiation of 20 ms in Ar atmosphere at pressures of 0.02, 0.05, and 0.1 MPa [29, 30]. The temperatures of growing clusters and/or condensing NPs, which existed at the front edges of laser plumes, were estimated by assuming blackbody radiation at various times after the start of laser irradiation. As a result, the fall rates of the temperatures were estimated to be 317, 235, and 199 K/s at Ar pressures of 0.02, 0.05, and 0.1 MPa. By assuming temperature ranges of 2200–1400 and 1400–800 °C for efficient growth of carbon nanohorns at 0.1 MPa and NTs at 0.05 MPa, the times available for the growth of the nanohorns and NTs were estimated to be 4.0 and 2.7 ms, respectively. Although the initial temperature of ejected Ge and Si species and the temperature range contributing SiO_x NT growth is not clear, we assume a growth-temperature range of 1500–500 °C according to the melting point of 938.25 °C of bulk Ge and the heating temperatures used for SiO_x NTs growth (such as 950 [7] 1350 [9], and 1400 °C [5, 6]) in previous studies. By using the temperature fall rates of 235 and 199 K/s, the times available for the growth of the SiO_x NTs can be estimated to be 4.3 and 5.0 ms at 0.05 and 0.1 MPa. Since much smaller temperature fall is expected at a higher pressure of 0.9 MPa, if we assume a fall rate of 50 K/s, the time available for the NT growth is 20.0 ms. In previous

studies leading to the growth of very long NTs, heating Si and indium oxide powders was carried out at ~ 1400 °C for 40 min to produce NTs of 0.9–1.0 mm [6], and heating of Fe/Co/Ni alloy NPs with Si powders was carried out in Ar/H_2 gas at 1350 °C for 2 h producing NTs of 100 µm or more [9]. The estimated times of 4.3–20.0 ms in this study are significantly short and consistent with the grown NTs with short lengths up to only ~ 3 µm. The growth process of SiO_x NTs involving the oxidation of Si should also be ruled out.

4 Conclusions

We carried out laser vaporization of a Ge/Si target (Si content: 5 at.%) at Ar pressures of 0.01–0.9 MPa. A maximum amount of 1D nanostructures (~ 30% of all products) was produced together with many NPs as deposits at 0.9 MPa. The 1D nanostructures were identified as amorphous SiO_x NTs and attached with crystalline Ge-rich NPs having elongated prolate- and sphere-like shapes at their tips. The average diameters and wall thicknesses were 51.6 and 12.6 nm for the NTs attached with prolate-like NPs and 64.1 and 13.7 nm for the NTs attached with sphere-like NPs. As the Ar pressure decreased from 0.9 to 0.03 MPa, the average diameters, wall thicknesses, and lengths of the NTs decreased and the average tip NP sizes decreased. There was a strong correlation among the average diameters, wall thicknesses, and lengths of the NTs and the average sizes of the tip NPs, indicating the catalytic role of molten Ge NPs for the precipitation of SiO_x in a VLS growth mechanism at high temperature. The evaluation of SiO_x precipitation quantities from seed Ge NPs for NT growth was carried out to compare those quantities with those in the SiO_x NWs grown by laser vaporization of Si at Ar pressures of 0.1, 0.5, and 0.9 MPa. The NT volumes per tip NP volume were 1.2×10^{-3}–1.0×10^{-2} of those of the NWs. We concluded that small SiO_x precipitation quantities play a critical role in NT growth from molten Ge NPs with different shapes and sizes. Further investigation is still required to understand the growth process of NTs such as how to separate SiO_x sheaths from supersaturated Ge-rich molten NPs with different sizes and curvatures under the condition of small precipitation quantities. The nanostructures, NTs and NPs composed of Si, O, and Ge atoms, obtained in this study may find applications as high-performance anode materials for rechargeable lithium ion batteries [15, 16].

Compliance with ethical standards

References

1. Nakamura H, Matsui Y (1995) Silica gel nanotubes obtained by the sol–gel method. J Am Chem Soc 117:2651–2652
2. Yang X, Tang H, Cao K et al (2011) Templated-assisted one-dimensional silica nanotubes: synthesis and applications. J Mater Chem 21:6122–6135
3. Zhang W, Hong C, Pan C (2014) Fabrication and characterization of silica nanotubes with controlled dimensions. J Mater Chem A 2:7819–7828
4. Farid G, Kruk M (2017) Silica nanotubes with widely adjustable inner diameter and ordered silicas with ultralarge cylindrical mesopores templated by swollen micelles of mixed pluronic triblock copolymers. Chem Mater 29:4675–4681
5. Wang ZL, Gao RP, Gole JL et al (2000) Silica nanotubes and nanofiber arrays. Adv Mater 12:1938–1940
6. Li Y, Bando Y, Golberg D (2004) Indium-assisted growth of aligned ultra-long silica nanotubes. Adv Mater 16:37–40
7. Liang C, Shimizu Y, Sasaki T et al (2004) One-step growth of silica nanotubes and simultaneous filling with indium sulfide nanorods. J Mater Chem 14:248–252
8. Hu J, Jiang Y, Meng X et al (2005) Temperature-dependent growth of germanium oxide and silicon oxide based nanostructures, and silicon oxide microtubes. Small 4:429–438
9. Jiang Z, Xie T, Yuan XY et al (2005) Catalytic synthesis and photoluminescence of silicon oxide nanowires and nanotubes. Appl Phys A 81:477–479
10. Esterina R, Liu XM, Ross CA et al (2012) Synthesis of silicon oxide nanowires and nanotubes with cobalt–palladium or palladium catalysts. J Appl Phys 112:24312
11. Tuan H, Ghezelbash A, Korgel BA (2008) Silicon nanowires and silica nanotubes seeded by copper nanoparticles in an organic solvent. Chem Mater 20:2306–2313
12. Kokai F, Shimazu T, Adachi K et al (2009) Fabrication of completely filled carbon nanotubes with copper nanowires in a confined space. Appl Phys A 97:55–62
13. Kokai F, Uchiyama K, Shimazu T et al (2010) Fabrication of two types of one-dimensional Si–C nanostructures by laser ablation. Appl Phys A 101:497–502
14. Kokai F, Inoue S, Hidaka H et al (2013) Catalyst-free growth of amorphous silicon nanowires by laser ablation. Appl Phys A 112:1–7
15. Kobayashi K, Kokai F, Sakurai N et al (2013) Silicon-catalyzed growth of amorphous SiO_x nanowires by laser vaporization of Si and Si/SiO_2. J Phys Chem C 117:25169–25174
16. Kokai F, Sawada N, Hatano K et al (2018) Silicon-catalyzed growth of amorphous SiO_x nanowires by continuous-wave laser ablation of SiO in high-pressure gas. Appl Phys A 124:40
17. Hatano K, Asano Y, Kameda Y et al (2017) Formation of germanium–carbon core–shell nanowires by laser vaporization in high-pressure Ar gas without the addition of other metal catalysts. Mater Sci Appl 8:838–847
18. Kokai F, Takahashi K, Yudasaka M et al (1999) Emission imaging spectroscopic and shadowgraphic studies on the growth dynamics of graphitic carbon particles synthesized by CO_2 laser vaporization. J Phys Chem B 103:8686–8693
19. Guo T, Nikolaev P, Thess A et al (1995) Catalytic growth of single-walled nanotubes by laser vaporization. Chem Phys Lett 243:49–54
20. Morales AM, Lieber CM (1998) A laser ablation method for the synthesis of crystalline semiconductor nanowires. Science 279:208–211
21. Briggs D, Seah MP (1988) Practical surface analysis by auger and X-ray photoelectron spectroscopy. Wiley, Chichester, p 499
22. Terrasi A, Scalese S, Adorno R et al (2002) Rapid thermal oxidation of epitaxial SiGe thin films. Mater Sci Eng B 89:269–273
23. Briggs D, Seah MP (1988) Practical surface analysis by auger and X-ray photoelectron spectroscopy. Wiley, Chichester, p 488
24. Chastain J, King RC Jr (1992) Handbook of X-ray photoelectron spectroscopy. ULVAC-PHI, Inc, Chigasak, p 231
25. Wagner CD, Zatko DA, Raymond RH (1980) Use of the oxygen KLL Auger lines in identification of surface chemical states by electron spectroscopy for chemical analysis. Anal Chem 52:1445–1451
26. Alonso ML, Winer K (1989) Raman spectra of c-$Si_{1-x}Ge_x$ alloys. Phys Rev B 39:10056–100062
27. Lu Q, Adu KW, Gutiérrez HR et al (2008) Raman scattering from $Si_{1-x}G_x$ alloy nanowires. J Phys Chem 112:3209–3215
28. Koren G, Oppenheim UP (1987) Laser ablation of polymers in pressurized gas ambients. Appl Phys B 42:41–43
29. Kokai F, Takahashi K, Kasuya D et al (2001) Growth of single-walled carbon nanotubes dependent on laser power density and ambient gas pressure during room-temperature CO_2 laser vaporization. Appl Phys A 73:401–407
30. Kokai F, Takahashi K, Kasuya D et al (2002) Growth dynamics of single-walled carbon nanotubes and nanohorn aggregates by CO_2 laser vaporization at room temperature. Appl Surf Sci 197–198:650–655
31. Masuda S, Takagi K, Dong W et al (2008) Solidification behavior of falling germanium droplets produced by pulsated orifice ejection method. J Cryst Growth 310:2915–2922
32. Hofmann S, Sharma R, Ducati C et al (2007) In situ observations of catalyst dynamics during surface-bound carbon nanotube nucleation. Nano Lett 7:602–608
33. Schmidt V, Wittemann JV, Senz S et al (2009) Silicon nanowires: a review on aspects of their growth and their electrical properties. Adv Mater 21:2681–2702
34. Lide DR (2008) CRC handbook of chemistry and physics, 88th edn. CRC Press, Boca Raton, pp 9-56–9-60